Device

Article

A stretchable optical-fiber-like triboelectric sensor for monitoring large-scale cable structures

Graphical abstract

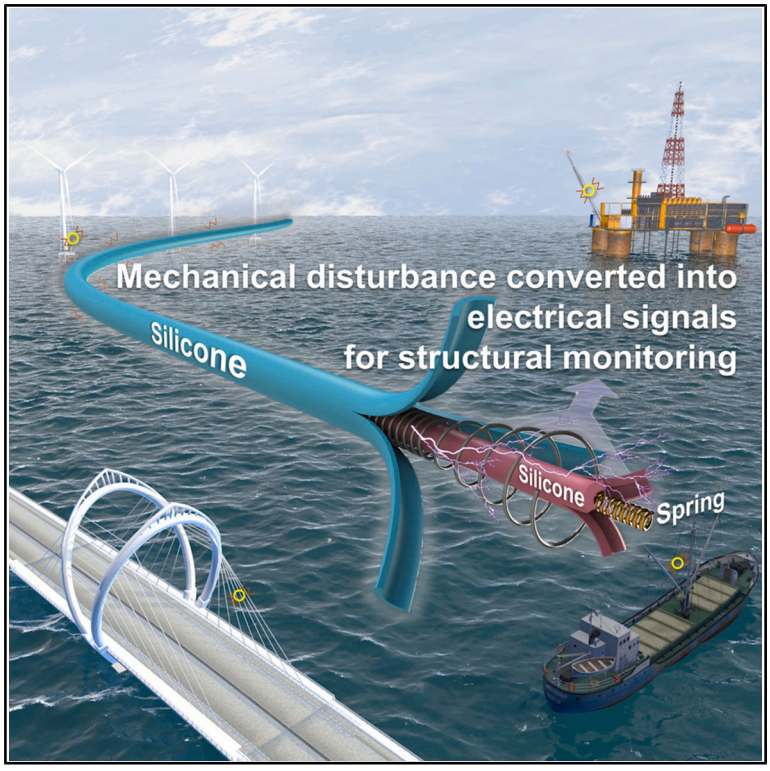

Highlights

- A fiber-inspired sensing cable is designed for monitoring cable structures
- Coaxial sensor enables dual-modal sensing of cable tension and vibration
- Sensor shifts from discrete local sensing to spatially integrated perception
- Multi-functional sensing spans tension, vibration, and fault monitoring

Authors

Hengxu Du (杜恒旭), Ziyue Xi (席子岳), Mengwei Wu (吴梦维), ..., Han Yan (严寒), Hongyong Yu (于洪勇), Minyi Xu (徐敏义)

Correspondence

wumengwei@dlmu.edu.cn (M.W.), yuhongyong2020@dlmu.edu.cn (H.Y.), xuminyi@dlmu.edu.cn (M.X.)

In brief

Du et al. present a stretchable optical-fiber-like triboelectric sensor (SOFTS) for structure-wide cable monitoring. The elastic coaxial structure enables stable operation under deformation and converts distributed mechanical excitations into a unified electrical signal. The sensor enables long-term and real-time monitoring of tension, vibration, and structural conditions in cables.

Explore
Early prototypes with exciting performance and new methodology

Du et al., 2026, Device *4*, 101079
April 17, 2026
https://doi.org/10.1016/j.device.2026.101079

CellPress

Please cite this article in press as: Du et al., A stretchable optical-fiber-like triboelectric sensor for monitoring large-scale cable structures, Device (2026), https://doi.org/10.1016/j.device.2026.101079

Device

CellPress

Article

A stretchable optical-fiber-like triboelectric sensor for monitoring large-scale cable structures

Hengxu Du (杜恒旭),[1,3] Ziyue Xi (席子岳),[1,3] Mengwei Wu (吴梦维),[1,*] Yan Yang (杨焱),[1] Yawei Wang (王雅巍),[2] Guobiao Hu (胡国标),[2] Han Yan (严寒),[1] Hongyong Yu (于洪勇),[1,*] and Minyi Xu (徐敏义)[1,4,*]

[1]Dalian Key Lab of Marine Micro/Nano Energy and Self-powered System, Dalian Maritime University, Dalian 116026, Liaoning, China
[2]Thrust of Internet of Things, The Hong Kong University of Science and Technology (Guangzhou), Guangzhou 511455, Guangdong, China
[3]These authors contributed equally
[4]Lead contact
*Correspondence: wumengwei@dlmu.edu.cn (M.W.), yuhongyong2020@dlmu.edu.cn (H.Y.), xuminyi@dlmu.edu.cn (M.X.)
https://doi.org/10.1016/j.device.2026.101079

THE BIGGER PICTURE Cable-supported structures are infrastructure lifelines that require long-term monitoring of complex stress factors. Individual sensors can only provide localized data, and, while fiber-optic systems enable distributed sensing, their brittleness and limited stretchability restrict performance under the high mechanical loads and deformations in structural cable systems. Most existing flexible solutions are designed for small-scale applications or localized monitoring, struggling to match the dimensions of engineering structures, and achieving structure-wide, continuous perception remains a challenge. In this work, we designed a stretchable optical-fiber-like triboelectric sensor to bridge these gaps for large-scale cable monitoring.

SUMMARY

Cable structures require tension and vibration monitoring to ensure safety. While various flexible sensors and rope-like triboelectric nanogenerators have been developed to accommodate mechanical deformations, they typically rely on dense sensor arrays for large-scale coverage and lack the ability to integrate continuous signals. Here, we present a stretchable optical-fiber-like triboelectric sensor (SOFTS) for monitoring tension and vibration in large-scale cable structures. The sensor has a multi-layer coaxial structure with spring electrodes and silicone tubes, maintaining stable output under tensile strains exceeding 175% and converting mechanical excitations into electrical responses. Integrated with a one-dimensional convolutional neural network, the sensor achieves recognition accuracies of 98.69% for bridge structural deformation and 97.18% for cable damage detection.

INTRODUCTION

Cable structures are widely employed in bridges, towers, offshore platforms, elevators, and large lifting equipment. As key components that bear primary loads and transmit forces, their mechanical properties determine structural safety and stability. However, during long-term service, these structures are subjected to external factors such as stress loads, vibrations, temperature fluctuations, and material aging. Real-time monitoring of cable static tension and structural health is essential to ensure the safe operation of large-scale engineering structures.

Currently, cable-monitoring techniques primarily rely on point sensors (such as strain gauges,[1,2] piezoelectric sensors,[3,4] and accelerometers[5,6]) and distributed fiber-optic sensing technologies. Point sensors can capture localized responses with high precision, but their spatial coverage is limited, making it challenging to achieve continuous monitoring along the entire cable length. In contrast, fiber-optic sensors, represented by fiber Bragg grating[7] and distributed Rayleigh[8] or Brillouin backscattering[9] systems, enable distributed or quasi-distributed measurements by analyzing light scattering or wavelength shifts along the fiber, thereby achieving continuous detection of strain, temperature, and vibration over long distances.[10] Despite their sensitivity and spatial resolution, optical fibers suffer from brittleness and limited tensile flexibility,[11] which hinder operation under complex loading or large-deformation conditions. They also rely on external light sources and demodulation units, resulting in increased installation costs and system complexity.[12] In addition, cross-sensitivity between temperature and strain in

Please cite this article in press as: Du et al., A stretchable optical-fiber-like triboelectric sensor for monitoring large-scale cable structures, Device (2026), https://doi.org/10.1016/j.device.2026.101079

these optic fibers requires additional interrogation modules,[13] further constraining their deployment (Table S1).

Triboelectric nanogenerators (TENGs) provide an alternative solution in self-powered motion monitoring,[14,15] with advantages such as extensive material selection and adaptability to low-frequency and disordered motions.[16,17] TENGs operate based on the coupled effects of triboelectric charging and electrostatic induction, enabling conversion of mechanical energy into electrical energy. This facilitates passive mechanical-response detection. Leveraging the high structural design flexibility and broad material availability of TENGs, researchers have developed flexible, stretchable, and high-sensitivity rope-like TENGs.[18] These flexible, stretchable TENGs hold promise in applications such as wearable devices[19–33] and structural health monitoring.[34,35] With the integration of machine-learning and signal-processing algorithms, rope-like TENGs have demonstrated potential in localized sensing and small-scale motion monitoring.[20,27,35,36] However, most rope-like TENGs are installed by locally attaching fabric woven from fibers. For structural monitoring of longer cables, such designs struggle to integrate with the scale of target structures. Some research has proposed coaxial-structured TENGs that more closely resemble cable-like configurations.[21,37,38] However, their output signals primarily originate from localized responses, lacking the ability for spatially integrated sensing across the full span of large-scale engineering structures. In existing reports, rope-like TENGs function as locally attached sensors, where the electrical output reflects deformation at specific positions rather than the mechanical state of the rope or cable as an integrated structure.

Inspired by the structure-wide perception characteristics of optical fibers, we designed a stretchable optical-fiber-like triboelectric sensor (SOFTS) that mimics the continuous perception mechanism of optical fibers while maintaining mechanical flexibility, stretchability, and self-powered capability. The SOFTS employs a composite design of a double-layer coaxial spring and a flexible silicone tube, forming a multi-layer nested structure that can be continuously fabricated. The interaction between flexible silicone and metal springs endows the sensor with over 175% stretchability and bending resistance, enabling it to respond to stretch impact loads while detecting vibration signals. Drawing inspiration from fiber-optic deployment principles, SOFTS sensing units are distributed along the entire cable length. This configuration converts dynamic responses from different spatial locations into superimposed electrical signals, expanding discrete-point monitoring into continuous-line monitoring. Integration with convolutional neural network (CNN) algorithms enables recognition of the cable and the target structure. We applied the SOFTS to vibration and cable force monitoring of bridge stay cables. Results demonstrate that the SOFTS outputs electrical signals correlated with cable force and vibration frequency and achieves full-length signal integration under multi-point excitation conditions. By integrating CNN for extraction and recognition of the time-frequency characteristics of SOFTS output signals, classification of various operational conditions (e.g., structural damage, abnormal cable vibrations) is achieved. SOFTS differs from existing designs by integrating the triboelectric sensing mechanism with the load-bearing rope itself, enabling spatially coupled electromechanical responses along the cable. This structural integration facilitates cable-scale motion monitoring and supports damage-related feature analysis.

RESULTS AND DISCUSSION

Design and working mechanism of SOFTS

Figure 1A illustrates the structural schematic of SOFTS, which consists of two coaxially arranged spring electrodes and two layers of silicone tubing. The inner spring is coated with the inner silicone tube, heat-shrunk into shape, threaded through the outer spring, and encapsulated by the outer silicone tube before undergoing a second heat-setting process. The outer silicone tube encapsulation shields SOFTS from interference by external charged objects, ensuring signals are isolated for detecting external mechanical motion. The continuous sensing capability of SOFTS enables mechanical motions at different locations along the cable to be integrated into a unified electrical signal.

Figure 1B illustrates the voltage signal waveform generated when it vibrates after sudden stretch loading. Leveraging this signal characteristic, SOFTS converts mechanical motion in cable-like structures into electrical signals. Through signal acquisition and data training, it enables monitoring of cable structural health (as shown in Figure 1C). All components of SOFTS are fabricated from common flexible stretchable materials, enabling continuous fabrication and withstanding knotting, bending, and recoverable stretching deformations exceeding 175% (Figure 1D). Figure 1E displays scanning electron microscopy (SEM) images of the surfaces of the springs and silicone tubes.

The working mechanism of the SOFTS for electricity generation is governed by the coupling effect of contact electrification and electrostatic induction. The operational principle of the SOFTS under stretch loading is illustrated in Figures 1F and S1. In the initial state, negative static charges are distributed on the silicone surface, while the spring electrodes carry an equal number of positive charges. During the stretching and releasing process, the variation in the length of the SOFTS causes changes in the thickness and diameter of the silicone layer. Meanwhile, the pitch of the springs increases, whereas their diameters remain nearly constant. This results in a periodic contact-separation process between the inner silicone tube and the outer spring electrode, leading to a potential difference between the two spring electrodes. Under short-circuit conditions, electrons migrate through the external circuit between the two electrodes to balance the potential difference, generating an output current.

The gap between the silicone and spring electrodes enables it to respond to radial mechanical vibrations. As shown in Figures 1F and S1, in the initial configuration, the spring electrodes are coaxially aligned with the silicone tubes. The relative position between the inner spring and the inner silicone tube remains unchanged; however, under external vibration excitation, they deviate from coaxial alignment with the outer spring and outer silicone tube. The inner spring and the inner silicone tube oscillate within the outer layers. The resulting contact separation between the inner silicone tube and the outer spring again

Please cite this article in press as: Du et al., A stretchable optical-fiber-like triboelectric sensor for monitoring large-scale cable structures, Device (2026), https://doi.org/10.1016/j.device.2026.101079

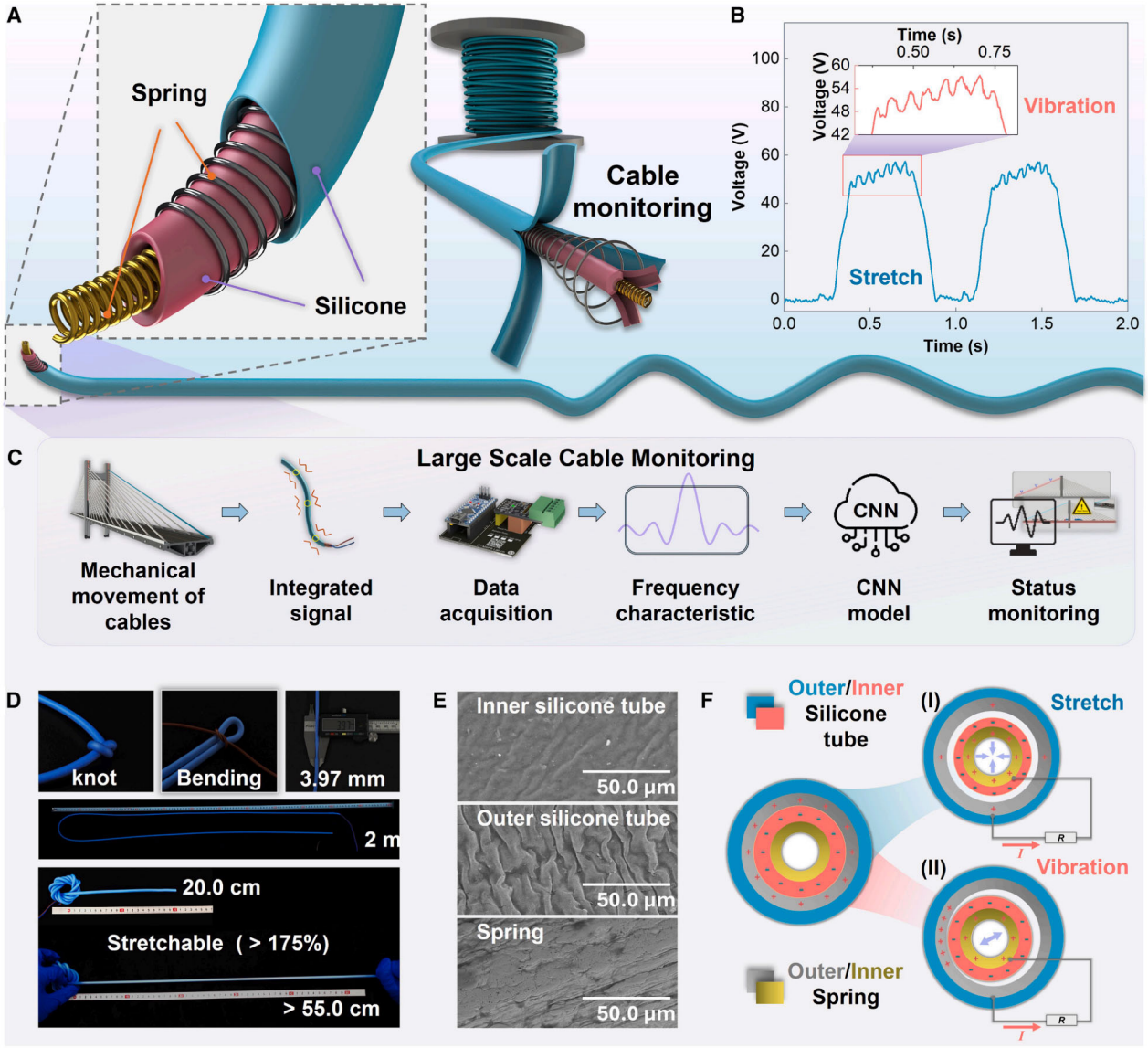

Figure 1. Design, features, and perception principles of SOFTS

(A) The structural design of SOFTS.

(B) SOFTS exhibits sensitive response to stretching and vibration.

(C) SOFTS's intelligent perception system.

(D) Dimensions, flexural strength, and stretch properties of SOFTS.

(E) SEM images of the springs and silicone tubes.

(F) The working principle of the SOFTS.

induces a potential difference, which generates the electrical signals under vibrational excitation.

Electromechanical response under stretch excitation

We investigated the electrical-output behavior of the device under stretch excitation. As illustrated in Figure 2A, SOFTS with an original length of L_0 was mounted on a linear motor (Figures 2B and S4) and stretched to a length L. The initial elongation rate (ε) was defined, where the elongation distance driven by the linear motor was denoted as ΔL. During stretching, electrical energy is produced through contact-separation interactions in the gap between the inner silicone tube and the outer spring. To investigate the effect of this gap on the output voltage, a detailed analysis was performed. Figure 2C shows the cross-sectional structure of SOFTS. In the experiments, outer springs with wire diameters of 0.3, 0.4, and 0.5 mm were employed, all possessing an outer diameter of 3.0 mm. A smaller wire diameter corresponds to a greater gap between the outer spring and the inner silicone tube.

Please cite this article in press as: Du et al., A stretchable optical-fiber-like triboelectric sensor for monitoring large-scale cable structures, Device (2026), https://doi.org/10.1016/j.device.2026.101079

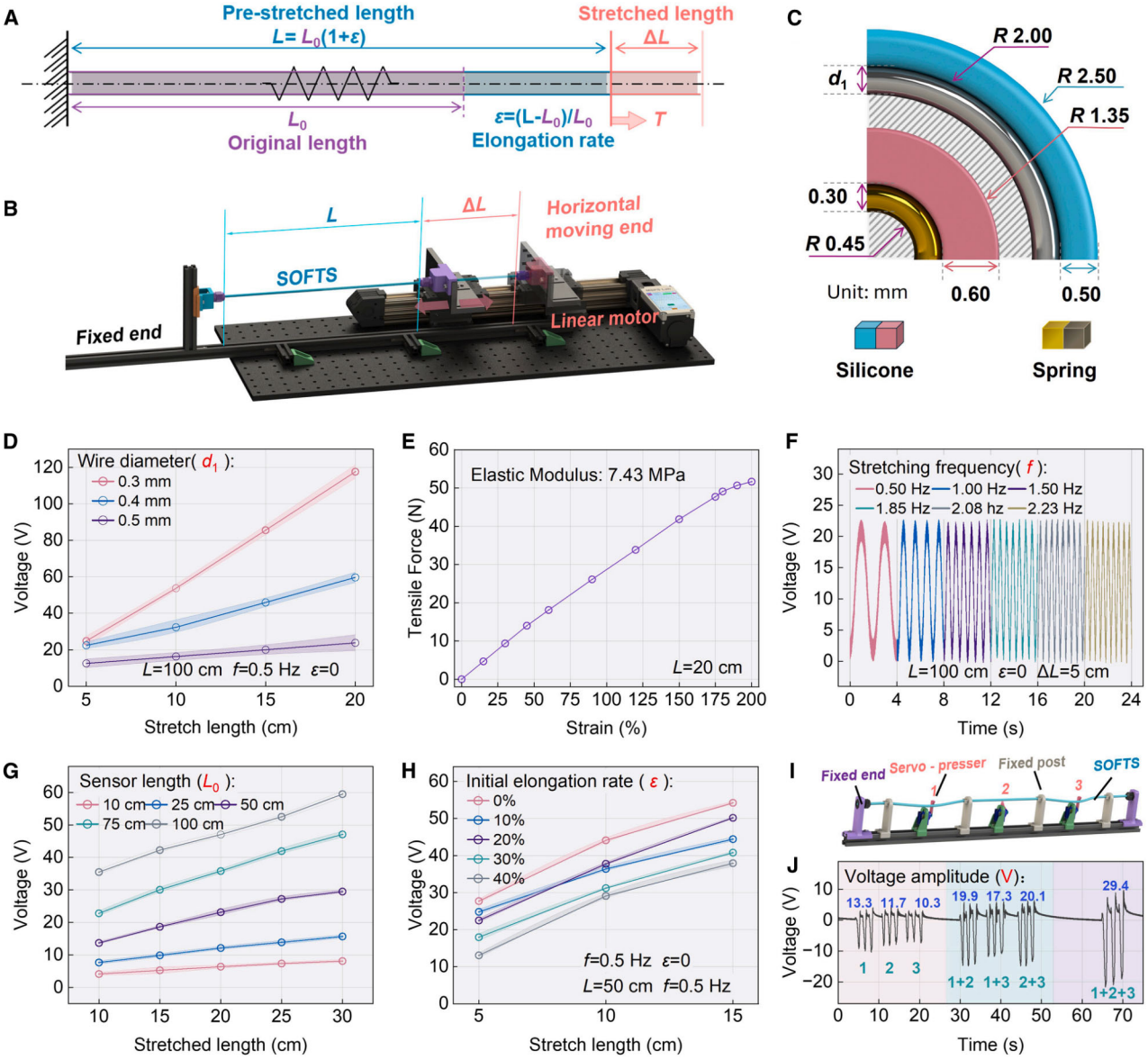

Figure 2. Output characteristics of SOFTS under stretch excitation

(A) Schematic diagram of parameters in stretch testing.
(B) Stretch test bench.
(C) Schematic diagram of cross-section structure and dimensions of SOFTS.
(D) Open-circuit voltage of SOFTS using outer springs with three different wire diameters.
(E) Tensile stress-strain behavior of SOFTS.
(F) Voltage output waveform of SOFTS under different stretching frequency excitations.
(G) Voltage signal amplitudes generated by SOFTS with different lengths under stretch excitation.
(H) Voltage signal amplitudes generated by SOFTS under five different initial elongation rates.
(I) An experimental bench with multi-local point excitation.
(J) The voltage signal waveform when multiple local points are excited.

Figures 2D and S5 present the open-circuit voltage, current, and transferred charge of SOFTS fabricated with three different outer-spring-wire diameters, all having an original length (L_0) of 100 cm. The results show that a thinner outer spring provides a larger contact-separation gap, which enhances the output performance of the SOFTS. When the stretching frequency is 0.5 Hz, the pre-stretched length (L) is 100 cm, and ε is 0, the SOFTS generates an open-circuit voltage of approximately 117 V, higher than most rope-like TENG sensors. SOFTS maintains elastic deformation under stretching strains exceeding 175%,

Please cite this article in press as: Du et al., A stretchable optical-fiber-like triboelectric sensor for monitoring large-scale cable structures, Device (2026), https://doi.org/10.1016/j.device.2026.101079

with an elastic modulus of 7.43 MPa (Figure 2E). The effect of stretching frequency on the voltage output was investigated. As shown in Figure 2F, the voltage signal produced by the SOFTS reflects the stretching frequency, while the amplitude of the voltage is slightly affected by frequency variations. As depicted in Figure 2G, the voltage output during the stretching tests shows a positive correlation with both the L_0 and the stretched length (ΔL).

Before applying stretch excitation, stretch SOFTS to length L at rate ε. The relationships among parameters in stretch testing (ε, L_0 and L) are summarized in Table S2. The parameter ε determines the effective contact area participating in the contact-separation process. At the same L, a larger ε corresponds to a shorter effective length of the SOFTS involved in electricity generation. Consequently, a smaller initial strain leads to a higher voltage output, as illustrated in Figure 2H.

Because SOFTS generates a single, integrated electrical output in response to distributed mechanical stimuli, we investigated whether the electrical signals generated at different local points are superimposed in an integral-like manner. As illustrated in Figure 2I, a 100-cm-long SOFTS was fixed onto a support frame and partitioned into three regions by four fixed posts. In each region, a servo motor was used to apply three cycles of periodic pressure to induce localized stretch deformation. Figure 2J presents the voltage signals under different excitation conditions, corresponding from left to right to the activation of one, two, and three regions, respectively. The results indicate that the voltage amplitude increases with the number of regions being stimulated. While the enhancement does not follow linear superposition, the overall trend confirms that electrical signals generated from different local areas are integrated into a single, unified output rather than being canceled out. This integral-like coalescence behavior verifies the capability to convert multiple distributed excitations into a spatially integrated electrical response.

Electromechanical response under strike excitation

The second mode of SOFTS involves converting mechanical energy from vibration excitation into electrical energy. Cable structures typically serve as flexible connecting components, bearing tensile constraints from both end structures and local loads between them. Leveraging its flexibility, SOFTS can maintain synchrony with the dynamic motion of the cable. Its stretchable properties enable adaptation to deformations caused by dynamic cable force variations. For example, cable-stayed bridges exhibit periodic vibrations in their cables under vehicle loads and environmental excitation. For cable structures subjected to static tension, their natural frequency remains constant. Based on the cable's material properties and measured vibration frequency, the static tension can be calculated using the frequency method, assessing the cable's health status, as shown in Figure 3A.

In the monitoring of bridge cables, engineers usually use the tapping method to measure the natural vibration frequency of the cables and then use Equation 1 to calculate the cable tension. The more detailed calculation method is presented in Note S2. Therefore, once SOFTS detects the vibration frequency of the cable, the cable tension can be inversely calculated from the above equation. To verify the feasibility of SOFTS-based tension monitoring, a striking platform was established, as shown in Figure 3B. A servo motor equipped with a strike rod was used to apply single striking excitations to the SOFTS, while the motor could slide along a linear rail to adjust the striking position (Figure S6). After each strike, SOFTS underwent free vibration at its natural frequency and generated corresponding electrical signals. First, the response characteristics of SOFTS under different elongation rates were examined. The electrical signals recorded after striking are presented in Figure 3C. Frequency spectra of the signals obtained under five elongation-rate conditions (Figure 3D) reveal that the natural frequency of SOFTS increases with increasing elongation rate, and the modal frequency distribution exhibits a strong linear relationship. This observation demonstrates the capability of SOFTS for reliable, self-powered monitoring of cable tension.

$$T = \frac{4\rho L^2 f_n^2}{n^2} \qquad \text{(Equation 1)}$$

The servo motor was moved along the rail to strike different positions on the SOFTS. The corresponding frequency spectra of the electrical signals (Figures S7 and 4A) show that the SOFTS output signals are nearly identical in the frequency domain, indicating that the natural vibration frequency is independent of the striking position. Multiple strikes were applied at the same position (Figures S8 and 4B), and the results demonstrate that the generated electrical signal was consistent across repeated tests. These results indicate that, both in the temporal dimension (repeated strikes) and the spatial dimension (different striking positions), the SOFTS can capture the vibration frequency of the cable through its electrical response.

As shown in Figures 4C and S9, a cable-stayed bridge model was constructed in which one of the stay cables was replaced with SOFTS. A servo motor installed on the bridge deck (Figure S10) served as the striking actuator for the SOFTS. Based on this setup, an active-excitation-based cable-tension measurement system was designed. An analog-to-digital converter (ADC) circuit board was fabricated using an ADS1115 module and an Arduino Nano (Figure S11) to acquire the electrical signals generated by the SOFTS. A user interface (UI) was developed in PyCharm (Figure S12) to visualize the real-time waveforms of both time-domain and frequency-domain signals. A control button labeled "Press to Detect" was placed at the upper-right corner of the interface. When pressed, the host computer sent a control command to another Nano board to trigger a single striking action of the servo motor. During measurement, the button status changed to "Detecting" until the vibration signal completely disappeared. For practical cable-tension calculation, the parameters of the cable must be substituted and calibrated. A dynamometer was used to roughly measure the actual tension. The fitted relationship between tension and elongation rate was coupled with the relationship between frequency and elongation rate to establish the correspondence between tension and elongation rate. Video S1 shows the measurement performance of the system under different tension levels. Under five distinct tension conditions, the electrical signals collected from the SOFTS (Figure 4D) showed excellent agreement with the fitted curves (Figure 4E).

Please cite this article in press as: Du et al., A stretchable optical-fiber-like triboelectric sensor for monitoring large-scale cable structures, Device (2026), https://doi.org/10.1016/j.device.2026.101079

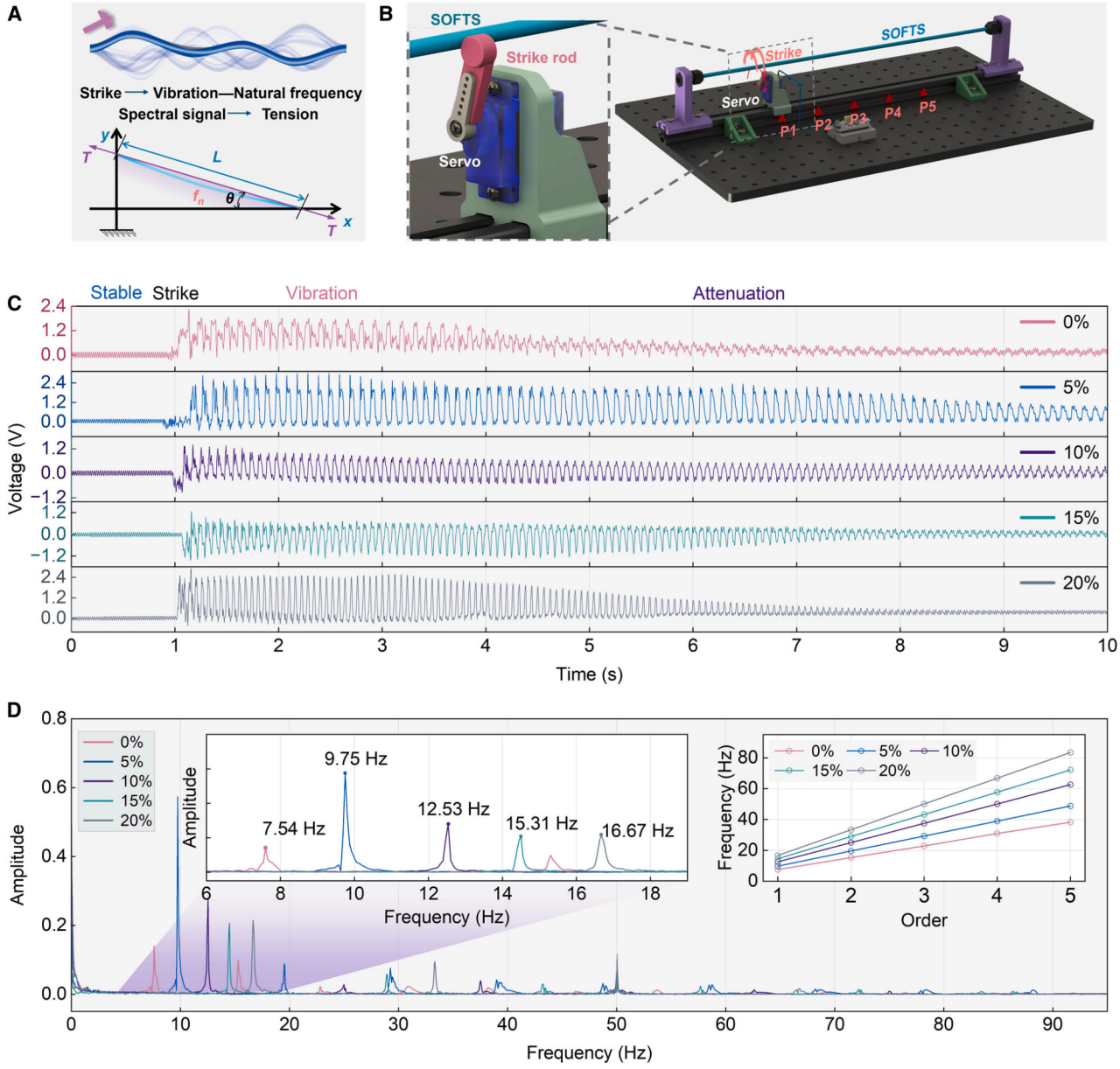

Figure 3. Output characteristics of SOFTS during strike-induced vibration

(A) Frequency method for measuring cable tension.

(B) Strike test bench.

(C) Voltage signal waveforms generated by the SOFTS under different stretching ratios during striking.

(D) Voltage signal spectra generated by the SOFTS under different stretching ratios during striking.

Electromechanical response under vibration excitation

Under fixed boundary constraints at both ends, the rope-like structure is prone to forced vibration induced by vibrations transmitted from the supporting structures and external excitations. When the external vibration frequency coincides with an integer multiple of its natural frequency, multiple vibration modes (*n*) are generated, producing electrical signals with distinct frequency characteristics (Figure 5A). To investigate the output behavior of SOFTS under different constraints, an experimental setup was constructed as shown in Figures 5B and S13. The SOFTS was fixed in various configurations and subjected to vibration excitation. The voltage output signals were analyzed when the SOFTS was excited vertically within the *xy* plane. The corresponding higher-order vibration modes of the SOFTS are displayed in Figure S14. In vibration mode, the interlayer gap also plays a role in the contact–separation

Please cite this article in press as: Du et al., A stretchable optical-fiber-like triboelectric sensor for monitoring large-scale cable structures, Device (2026), https://doi.org/10.1016/j.device.2026.101079

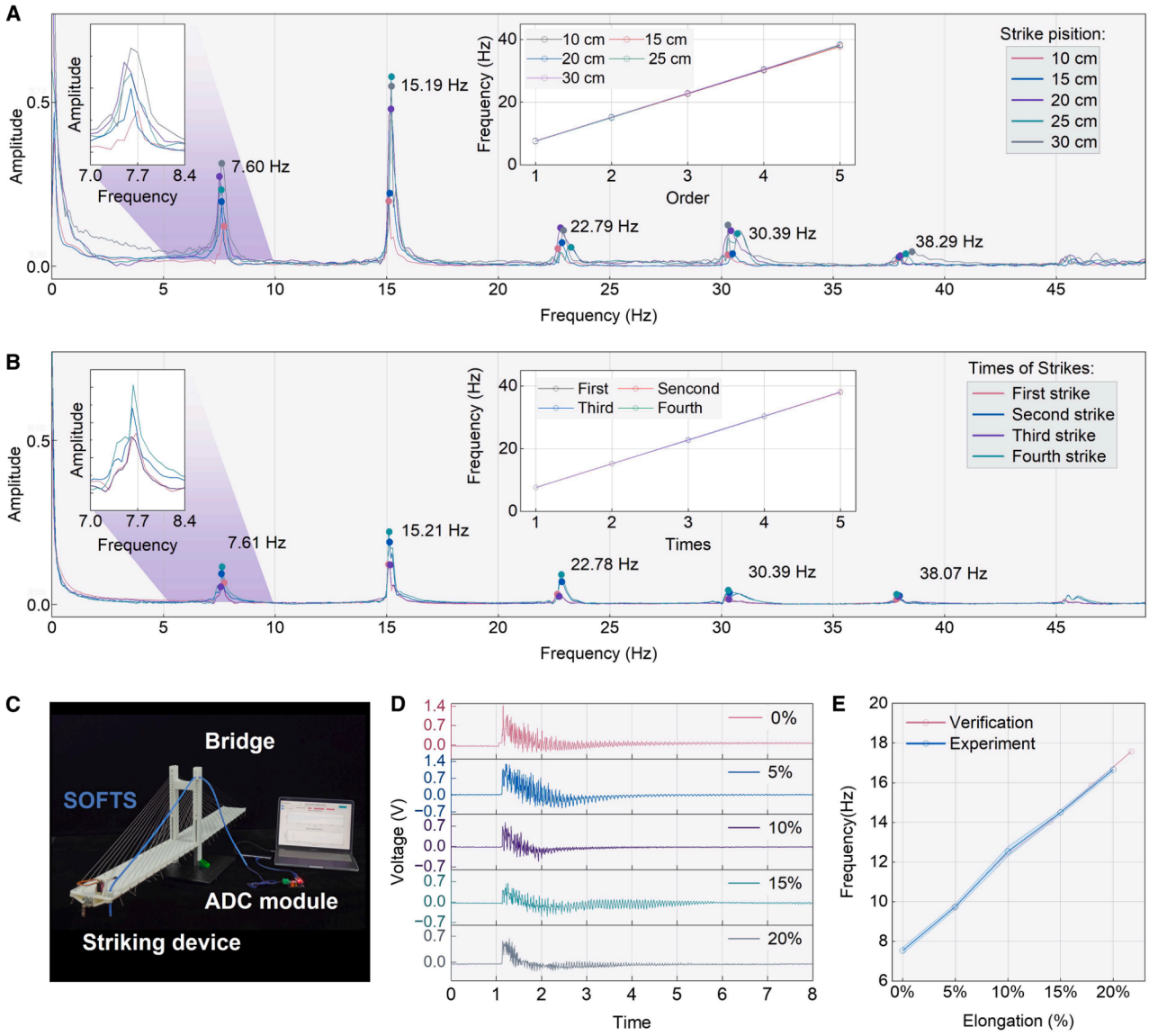

Figure 4. Demonstration of monitoring cable tension using sensors

(A) Voltage signal spectra generated by striking the SOFTS at different positions.

(B) Comparison of the voltage signal spectra produced by each strike on the SOFTS.

(C) Cable force monitoring test bench.

(D) The output signals of the SOFTS with different stretching ratios collected by the ADC module.

(E) Fitted relationship between cable force and frequency, and the cable force test results.

process. As shown in Figure 5C, SOFTS with thinner wire diameters exhibit larger contact-separation gaps, resulting in higher electrical output. Within the frequency range of 5–10 Hz, the SOFTS fabricated with three different outer springs produced their maximum output at 6 Hz. This is because 6 Hz is close to the natural frequency of the device, leading to intense first-order resonance for the given SOFTS length. The SOFTS accurately measures vibration excitations across a broad frequency range of 3–150 Hz (Figure S15) with a fitted slope of 0.994.

When the vibration frequency continues to increase and visible higher-order vibration modes are formed on the SOFTS, the voltage output reaches its maximum value. At this point, the corresponding frequency represents the higher-order vibration mode. To investigate the influence of resonance on the electrical response, tests were conducted over a wider frequency range. As shown in Figure 5D, the output voltage amplitudes of four SOFTS with different lengths were recorded under various vibration frequencies. Under vibration excitations ranging from 0 to 30 Hz, three vibration modes were observed across all four

Please cite this article in press as: Du et al., A stretchable optical-fiber-like triboelectric sensor for monitoring large-scale cable structures, Device (2026), https://doi.org/10.1016/j.device.2026.101079

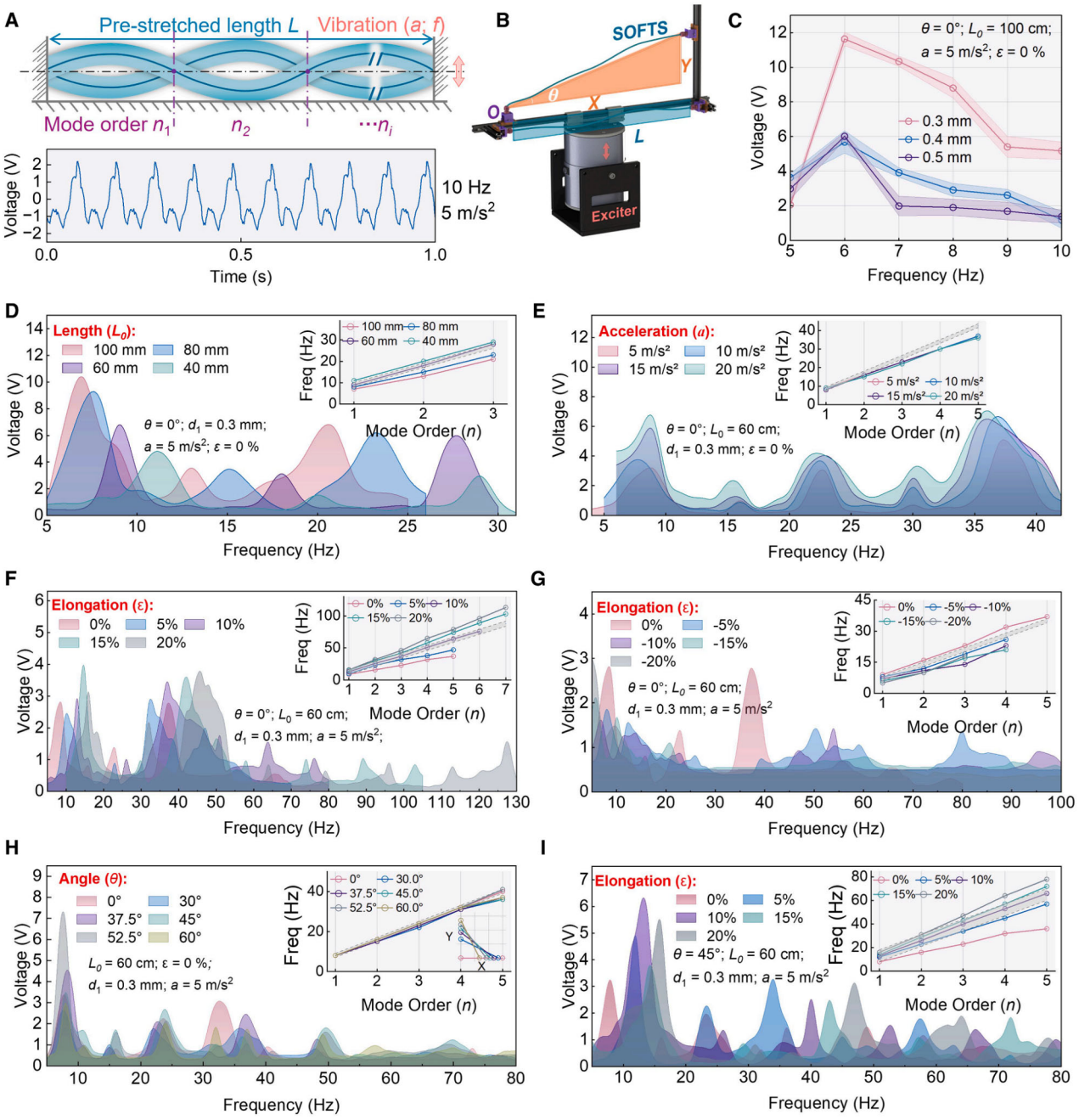

Figure 5. Output characteristics of the SOFTS during vibration with both ends constrained

(A) Schematic diagram of the vibration modes of the rope-like structure and the voltage signal waveforms generated by the SOFTS during vibration.
(B) Vibration test bench.
(C) Voltage of SOFTS using outer springs with three different wire diameters.
(D) Relationship between the voltage output amplitude and vibration frequency of SOFTS with different lengths.
(E) Relationship between the voltage output amplitude and vibration frequency of the SOFTS under different vibration accelerations.
(F) Relationship between the voltage output amplitude and vibration frequency of the SOFTS at different stretching ratios.
(G) Relationship between the voltage output amplitude and vibration frequency of the SOFTS in the relaxed state.
(H) Relationship between the voltage output amplitude and vibration frequency of the SOFTS installed at an inclined angle.
(I) Relationship between the voltage output amplitude and vibration frequency of the SOFTS installed at a 45°inclination under different elongation ratios.

Please cite this article in press as: Du et al., A stretchable optical-fiber-like triboelectric sensor for monitoring large-scale cable structures, Device (2026), https://doi.org/10.1016/j.device.2026.101079

SOFTS. The results indicate that a longer SOFTS produces a higher voltage output at resonance. Increasing the sensor length decreases the natural frequency, while the frequencies corresponding to higher-order modes exhibit shifts and are no longer integer multiples of the fundamental frequency. This deviation arises because, under fixed-end boundary conditions, the tensile deformation of the flexible structure alters its internal tension, introducing nonlinearity into the vibration modes. To explore this phenomenon, the vibration acceleration was increased. As illustrated in Figure 5E, when the acceleration was raised from 5 to 20 m/s^2, the stronger vibration amplitude enhanced the voltage output of the SOFTS. Although the frequencies corresponding to higher-order modes remained nonlinear, increasing the acceleration did not noticeably affect the modal frequency distribution for the same SOFTS.

This phenomenon is analogous to a tensioned string whose natural vibration frequency determines the tone it produces. The frequency of the string can be tuned by changing its effective length or by adjusting the tension, but it remains independent of the striking force. Inspired by this analogy, we investigated whether the electrical signals generated by the SOFTS could reflect the overall tension state of the cable. Table S3 presents the experimental parameters (ε, L_0, and L). As shown in Figure 5F, the natural frequency of the SOFTS increased with increasing elongation rate, and higher elongation facilitated the excitation of higher-order vibration modes. When the elongation rate was low (0% and 5%), the modal frequency points were distributed below the linear trend of harmonic multiples; when the elongation rate increased to 10%, the modal frequencies exhibited the best agreement with the theoretical linear relationship; as the elongation rate increased to 15% and 20%, the frequency distribution deviated from linearity, with modal points located above the linear trend. The flexibility and stretchability of the SOFTS enable its compatibility with various engineering cable structures. In rigid cables, it allows for high-precision linear vibration measurements, while its stretchable nature enables the simultaneous capture of strain-induced nonlinear dynamic responses when deformation occurs.

Following the preceding analyses, the SOFTS was adjusted to a relaxed state, as illustrated in Figure 5G. In this configuration, the voltage output amplitude decreased and exhibited no correlation with vibration frequency. This phenomenon occurs because a relaxed flexible rope offers greater degrees of freedom and energy dissipation, impeding the transfer of mechanical energy to the triboelectric layers. As a result, the efficiency of charge transfer is reduced, which in turn weakens the electrical output. To investigate the influence of installation angle, SOFTS was mounted on the vibration platform at various inclination angles for testing. As shown in Figure 5H, although minor fluctuations in voltage amplitude were observed at different angles, the overall modal distribution remained stable. Additional experiments were performed with the SOFTS installed at a 45° inclined and tensioned position while varying the elongation rate, as illustrated in Figure 5I. The results reveal that the modal distribution characteristics under different inclined-tension states are consistent with those of the horizontally mounted SOFTS.

A bridge vibration experiment was conducted to demonstrate the monitoring capability of the SOFTS. As shown in Figures 6A and S16, a cable-stayed bridge model equipped with a SOFTS was mounted on an exciter. The output electrical signals were collected using an ADC module, while an interactive interface developed in PyCharm was used for real-time visualization of both time- and frequency-domain waveforms. A commercial accelerometer was employed to monitor the vibration of the bridge model. As demonstrated in Video S2, the vibration frequencies measured by the SOFTS and the signal-acquisition system were in agreement with those obtained from the accelerometer. In addition, when the vibration frequency of the bridge model reached 10 Hz (close to the natural frequency of the SOFTS), strong resonance occurred. Once the system detected that the vibration frequency matched the resonance frequency, an alarm was triggered on the computer interface (Figure S17). Figures 6B and 6C show the time-domain waveforms and frequency spectra under resonant (10 Hz) and non-resonant (8 Hz) conditions, respectively. When the vibration amplitude exceeded the normal range but the frequency remained below resonance, the system issued an amplitude-anomaly warning once the voltage magnitude surpassed the preset threshold.

In this configuration, the static cable tension can be *in situ* monitored using the frequency method. Under extreme nonlinear vibration conditions, such as harsh environments or structural resonance, conventional tension-identification approaches relying on low-order modal frequencies are often incapable of representing the mechanical state of the cable. As demonstrated previously in Figure 2J, the output signal of the SOFTS exhibits a multi-point excitation superposition response. This characteristic implies that, when SOFTS is distributed along the entire length of a cable, it can integrate the distributed vibration information of the whole cable into a single composite electrical signal. Such a feature enables SOFTS to perform overall tension monitoring and provide higher-dimensional data support for identifying local cable damage, fatigue accumulation, or relaxation.

Structural monitoring with CNN integration

Compared with the existing large-scale rope-like triboelectric nanogenerators that focus on maximizing local electrical energy output or tensile sensitivity, SOFTS pays more attention to achieving spatially integrated signal collection at the cable scale. We introduced deep-learning techniques into the signal-recognition process. CNN, owing to its capability in time-frequency feature extraction and pattern recognition,[39] has been applied in vibration monitoring,[40,41] fault diagnosis,[42] and state recognition.[43,44] Here, we use CNN to analyze the output signals of SOFTS. By leveraging its ability to learn the time-frequency distribution characteristics of electrical signals, the system achieved identification and anomaly detection of cable operating states.

To realize feature extraction and state recognition of SOFTS output signals, a one-dimensional CNN-based signal recognition model was constructed. To ensure robust fault recognition, the raw time-series data are segmented using a sliding-window technique with a window size of 70 points and an overlap rate of 80%, ensuring signal continuity. These temporal segments

Please cite this article in press as: Du et al., A stretchable optical-fiber-like triboelectric sensor for monitoring large-scale cable structures, Device (2026), https://doi.org/10.1016/j.device.2026.101079

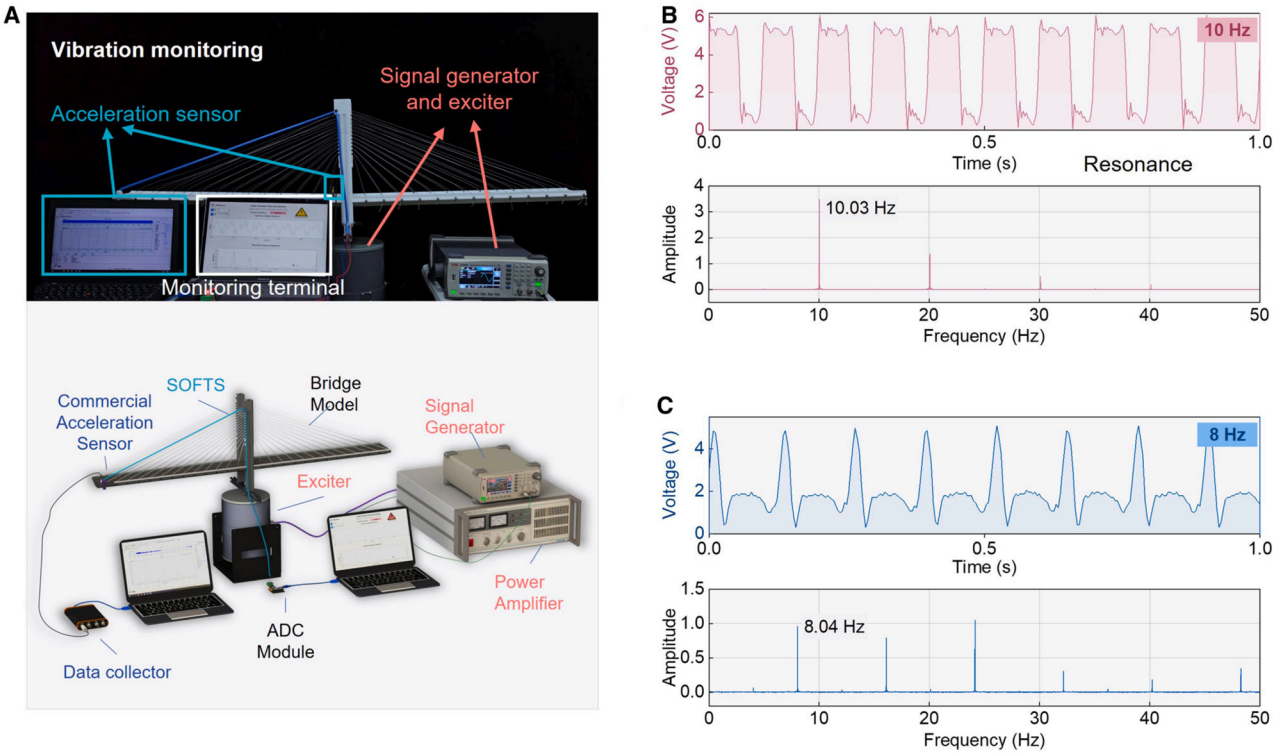

Figure 6. Application demonstration of the SOFTS for vibration monitoring

(A) Vibration monitoring test bench.

(B) Voltage output signals of the SOFTS when its natural frequency (10 Hz) matches the vibration frequency of the bridge model.

(C) The voltage output signal when SOFTS does not resonate with the bridge model.

are transformed into the frequency domain via fast Fourier transform, yielding 36 spectral features, which are standardized using *Z* score normalization. As illustrated in Figure 7A, the core classifier is a deep 1D-CNN composed of three hierarchical blocks. The first block utilizes 32 filters with a kernel size of 5 to capture broad spectral trends, while the subsequent two blocks employ 64 and 128 filters (with a kernel size of 3) to extract high-level abstractions. Feature dimensionality is progressively reduced using max-pooling in the initial layers, followed by adaptive average pooling in the final block to strictly enforce a fixed output feature dimension (128 $\times$ 16). To evaluate generalization capability, the dataset was randomly partitioned into training, validation, and testing sets with a ratio of 6:2:2, and the model was trained to minimize cross-entropy loss. By integrating the trained model with the SOFTS sensing unit, ADC module, and host computer terminal, a complete system was established enabling real-time signal visualization and online state recognition.

Five representative operating conditions were configured on the bridge model, as shown in Figures 7B and S18, corresponding to "normal vibration," "abnormal cable vibration," "overweight," "loosening," and "bridge damage" (Figure S19). The abnormal cable vibration condition was simulated by clamping an additional mass onto the cable to mimic localized damage. As main cables are the primary load-bearing components, such damage reduces the cross-sectional area and tensile strength. The overweight condition was generated by placing extra loads on the bridge deck; identifying this scenario is essential, as excessive vehicle loads accelerate fatigue accumulation and can cause deformation. The loosening condition referred to the relaxation of prestress at the anchorage end. Since the anchorage serves as a boundary condition, such loosening can lead to an uncontrollable redistribution of internal forces and potential structural instability. Finally, the bridge damage condition was simulated by removing the deck joint at the end of the deck segment to mimic structural degradation.

All tests were conducted under a 12-Hz excitation. Electrical signals were collected for 600 s using the ADC module at a sampling rate of 475 samples per second (SPS). The raw signal waveforms under the five operating conditions are presented in Figure 5C. The trained CNN model achieved a recognition accuracy of 98.69% in the multi-condition identification test (Figure 5D), demonstrating its capability in distinguishing between different vibration states of the cables and the bridge. Video S3 presents the real-time state-recognition process of the monitoring system. As displayed on the visualization interface (Figure S20), the acquired signal waveforms were updated in real time, while the CNN model performed condition classification and displayed the recognition results on the interface window.

Please cite this article in press as: Du et al., A stretchable optical-fiber-like triboelectric sensor for monitoring large-scale cable structures, Device (2026), https://doi.org/10.1016/j.device.2026.101079

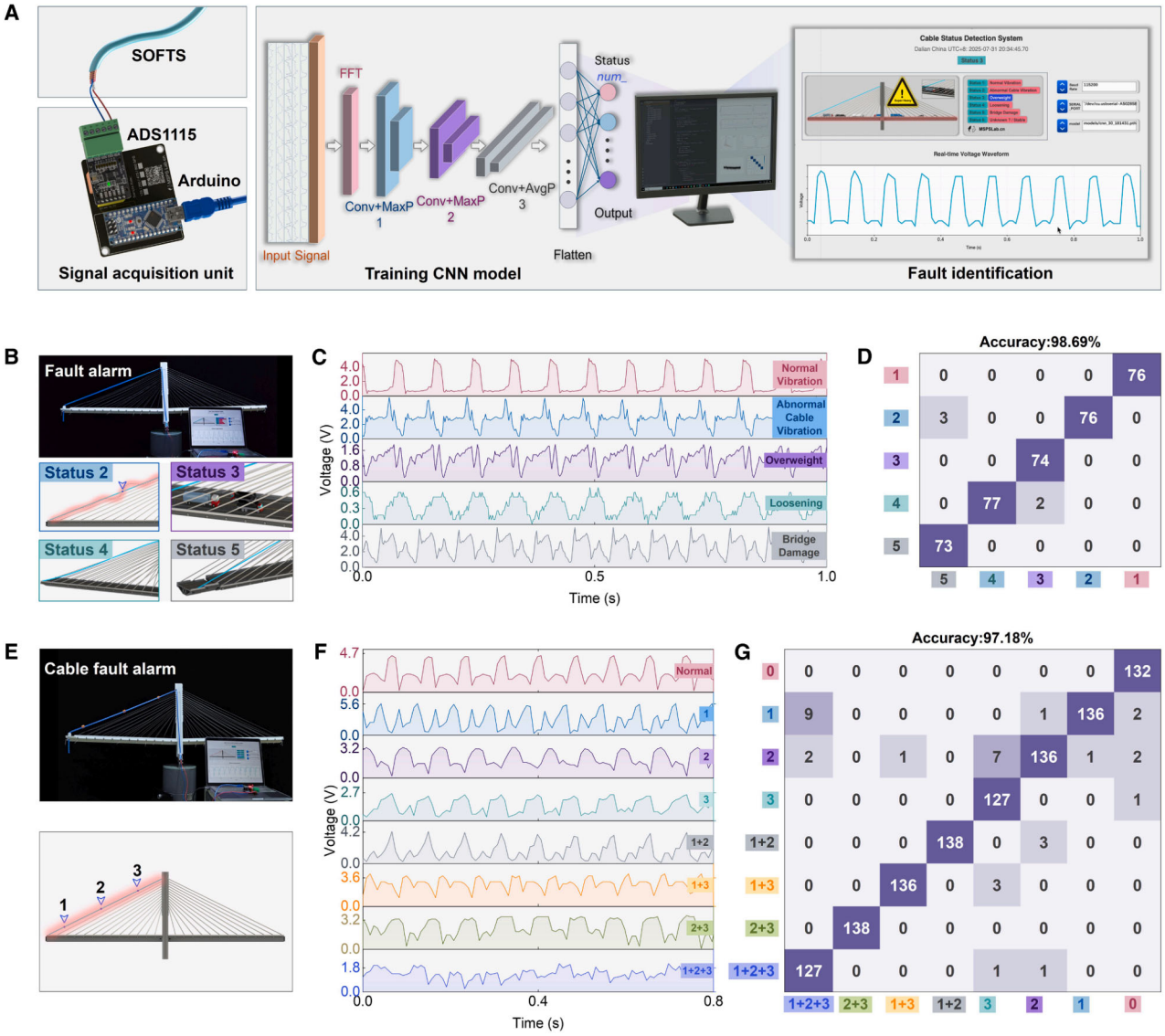

Figure 7. The demonstration of fault monitoring by SOFTS

(A) Schematic diagram of the SOFTS signal acquisition, data training, and working condition recognition system.
(B) Bridge model fault-monitoring test bench and demonstration of four fault conditions.
(C) Voltage signal waveforms of the SOFTS under five bridge-fault conditions.
(D) Confusion matrix of recognition accuracy for the five bridge-fault conditions.
(E) Cable-fault-monitoring test bench.
(F) Output signals of the SOFTS when cable faults are placed at different positions.
(G) Confusion matrix of recognition accuracy for the eight cable-fault conditions.

To validate the fiber-inspired perception concept, we extended the investigation from overall structural responses to localized damage scenarios, aiming to examine whether the integrated electrical output of SOFTS can distinguish spatial variations along the cable. To simulate local damage, additional masses were attached at three distinct positions along the cable (Figures 5E and S21). The selection of these locations was grounded in the structural mechanics of cable systems, targeting regions most susceptible to failure: "1" and "3" correspond to the anchorage zones (cable terminations at the bridge deck and tower), which are stress-concentration areas prone to loosening, corrosion, and fatigue cracking in engineering practice; meanwhile, "2" represents the mid-span region, a section typically experiencing maximum vibration amplitude and vulnerable to wind- and rain-induced fatigue or external impacts.

As shown in Figure 5F, SOFTS recorded electrical signals under eight different configurations (status 1–8), corresponding to varying numbers and positions of damage points. The trained CNN

Please cite this article in press as: Du et al., A stretchable optical-fiber-like triboelectric sensor for monitoring large-scale cable structures, Device (2026), https://doi.org/10.1016/j.device.2026.101079

model achieved a recognition accuracy of 97.18% for identifying the different clamping configurations (Figure 5G), and Video S4 illustrates the recognition performance of the model. Unlike conventional distributed sensors that offer inherent spatial resolution, SOFTS operates on a spatially integrated principle. It merges distributed mechanical excitations into a unified, single-channel voltage response. While this integration results in the loss of direct spatial coordinates in the raw signal, the distinct vibration modes caused by damage at different locations are encoded in the time-frequency domain, which can be decoded by the CNN.

Conclusions and outlook

We developed a SOFTS with full-length signal-integration capability. The cable integrates dual spring electrodes and multi-layer silicone tubes into a coaxial configuration, achieving flexibility, stretchability, and stable electrical output under large deformations. Its working mechanism, based on the coupling of contact electrification and electrostatic induction, enables the conversion of cable stretching, vibration, and impact into measurable electrical signals. Experimental results confirm that the voltage amplitude of the SOFTS increases with elongation, initial strain, and excitation frequency. Local mechanical excitations at different positions are spatially superimposed at the output, demonstrating an optical-fiber-like full-length response. Building on this mechanism, four representative applications were demonstrated, namely frequency-based tension monitoring using impact excitation, vibration monitoring and alerting, CNN-assisted fault recognition, and cable damage detection. SOFTS accurately captures cable tension and vibration modes, exhibiting repeatability across positions and excitations. Integrated with CNN, the system achieved recognition and visualization of various cable states, including normal vibration, overload, relaxation, and damage, achieving accuracy exceeding 98%. The combined use of SOFTS and CNN verifies its ability to decode spatially integrated signals and identify local damage, representing a fiber-like spatially resolved perception mechanism. SOFTS provides a low-cost, scalable, and fiber-inspired pathway for structure-wide health monitoring of bridges, marine cables, and other flexible large-deformation systems.

Several challenges remain for the practical long-term deployment of SOFTS. Unlike traditional fiber-optic sensors that utilize light with minimal attenuation over kilometers, SOFTS relies on triboelectric signals governed by contact electrification and electrostatic induction. The high impedance of triboelectric outputs makes the system susceptible to environmental electromagnetic interference and potential signal decay over long distances. While our experimental validations demonstrate stability at the meter scale, scaling this technology to the kilometer range required for maritime structures necessitate further validation. To ensure signal robustness, strategies such as multi-layer electromagnetic shielding and integrated impedance-matching circuits must be implemented. The integration of sensors into cables, followed by stringent encapsulation protocols and standardized industrial testing, also need to be optimized and tested before practical deployment. Future opportunities lie in integrating SOFTS with other technologies, such as fiber and external sensors, to realize distributed multi-functional and multi-scale monitoring (for example, to employ optical fibers to provide baseline environmental data while SOFTS captures transient triboelectric signals related to localized friction or impact).

METHODS

Three-dimensional models of some devices used in this work can be viewed via the QR code link in Document S1.

Fabrication of the SOFTS

The SOFTS is fabricated by coaxially nesting two silicone rubber tubes of different sizes with two 304 stainless-steel springs, followed by thermal molding. In this work, the inner silicone tube of red color is placed outside the inner spring for clear identification. The assembled unit is then passed through the outer spring and encapsulated by a blue outer silicone tube. An image of the molded SOFTS is presented in Figure S2. The two signal leads of the sensor are soldered to the inner and outer springs, respectively, and insulated to prevent electrical interference. SOFTS demonstrates good tolerance to humidity, and the electrical signal output remains stable within an air humidity range of 40%–80%, as shown in Figure S23. The underwater connector and 706 organic silicone sealant are used to ensure the stable output of SOFTS underwater. The finished SOFTS has a diameter of approximately 4 mm and a temperature-resistance range of -60°C to 200°C. After salt-spray testing and ultraviolet aging treatment, the silicone-gel encapsulation did not show obvious cracking, yellowing, or embrittlement (the detailed test conditions are described in Note S1) and the output voltage remained stable (Figure S24). As shown in Figure S2, a waterproof connector at each end is used as a clamping device, and various polylactic acid (PLA)-based brackets fabricated by 3D printing are employed to fix and mount the waterproof connectors.

Bridge model construction

In this work, the bridge model was designed based on the prototype of the Jinzhou wan bridge in Dalian, China. A scaled-down cable-stayed bridge model with a scale ratio of 200:1 was constructed, having a total length of 120 cm and a height of 36 cm, as shown in Figure S9. The main girder and base of the bridge were fabricated using 2020L aluminum profiles and angle brackets, while the bridge deck and connecting components were produced from 3D-printed PLA materials. The stay cables were made of 2-mm-diameter steel strands, with one end fixed to a 3D-printed connector on the main girder and the other end anchored by miniature steel-wire clamps embedded in the bridge deck. After installation, the cables were tensioned and secured with screws. The bridge decks were assembled using mortise-and-tenon joints, and lateral tension from the stay cables was utilized to prevent sagging of the overall structure.

Measurement

In the experimental measurements, the electrical signals of the SOFTS were recorded using a Keithley 6514 electrometer. For the application demonstrations, an Arduino Nano microcontroller and an ADS1115 ADC (sampling rate of 475 Hz, baud rate of 115200) were employed to acquire the output signals of the SOFTS. The ADC module, integrated on a custom-designed

printed circuit board (PCB) (Jialichuang EDA design), facilitated efficient real-time data collection. Both the photograph and circuit-design layout of the PCB module are presented in Figure S11.

Vibration excitation

In this work, a linear motor (model YDB65-LT-P400-L130-200-L3) was used to apply tensile excitation to the SOFTS, as shown in Figure S4. The SOFTS was fixed onto the linear motor through waterproof connectors and 3D-printed mounting brackets (Figure S3) to ensure stable mechanical coupling during the stretching tests.

For the impact experiments, a tapping rod was designed and mounted on an SG90 servo motor, as illustrated in Figure S6. An Arduino Nano microcontroller served as the control unit to regulate the tapping timing. The Arduino was connected to a computer host, allowing either scheduled tapping via preset timing or manual triggering through a button interface in PyCharm. The servo motor was installed on the bridge model or aluminum frame using 3D-printed brackets to ensure precise and repeatable impacts.

For the vibration experiments, an exciter (model JZK-50) was employed to simulate dynamic vibration. The excitation signal was generated by a signal generator (UTG2062B), amplified by a power amplifier (YE5874A), and subsequently fed into the exciter. An acceleration sensor (KS 96.100) was used to monitor the real-time vibration acceleration during the experiments. The complete vibration-testing setup is shown in Figure S13.

UI design

A UI design was developed in PyCharm using the PyQt framework to enable real-time signal monitoring and intelligent recognition. The interface provides real-time displays of time-domain and frequency-domain waveforms along with a real-time clock, a baud rate setting box, and serial port channel-selection options. It also includes a CNN model loading module, a manual excitation control button for the servo motor, and a visualization panel for recognition results. These integrated functions allow seamless communication between the hardware-acquisition module and the software-display system. The four corresponding monitoring interfaces are illustrated in Figures S12, S17, S20, and S22.

RESOURCE AVAILABILITY

Lead contact

Requests for further information, resources, and reagents should be directed to and will be fulfilled by the lead contact, Minyi Xu (xuminyi@dlmu.edu.cn).

Materials availability

This study did not generate new unique reagents.

Data and code availability

- The data used to support the findings of this study are available from the lead contact upon reasonable request.
- The code for sensor data acquisition and training methods is available at https://doi.org/10.5281/zenodo.18309823.

ACKNOWLEDGMENTS

This work was supported by the National Natural Science Foundation of China Youth Science Fund Project (no. 52501415); Beijing Key Laboratory of High-Entropy Energy materials and Devices, Beijing Institute of Nanoenergy and Nanosystems (no. GS2025MS005); and the Fundamental Research Funds for the Central Universities (no. 3132025227).

AUTHOR CONTRIBUTIONS

H.D., Z.X., and H. Yu contributed to the research conceptualization and methodology, conducted the experimental validation, and wrote and revised the original manuscript. Y.W., G.H., and H. Yan contributed to the fabrication of the device. Y.Y. contributed to the software programming. M.X., H. Yu, and M.W. supervised and performed project administration.

DECLARATION OF INTERESTS

The authors declare no competing interests.

SUPPLEMENTAL INFORMATION

Supplemental information can be found online at https://doi.org/10.1016/j.device.2026.101079.

Received: November 28, 2025
Revised: December 16, 2025
Accepted: February 3, 2026

REFERENCES

1. Ajovalasit, A. (2011). Advances in Strain Gauge Measurement on Composite Materials. Strain *47*, 313–325. https://doi.org/10.1111/j.1475-1305.2009.00691.x.
2. Huang, Y.H., Liu, L., Sham, F.C., Chan, Y.S., and Ng, S.P. (2010). Optical strain gauge vs. traditional strain gauges for concrete elasticity modulus determination. Optik *121*, 1635–1641. https://doi.org/10.1016/j.ijleo.2009.03.002.
3. Hadidi, S., and Hassanzadeh, A. (2023). A Novel Self-Powered, High-Sensitivity Piezoelectric Vibration Sensor Based on Piezoelectric Combo Effect. IEEE Sens. J. *23*, 25797–25803. https://doi.org/10.1109/JSEN.2023.3317445.
4. Hake, A.E., Zhao, C., Sung, W.-K., and Grosh, K. (2021). Design and Experimental Assessment of Low-Noise Piezoelectric Microelectromechanical Systems Vibration Sensors. IEEE Sens. J. *21*, 17703–17711. https://doi.org/10.1109/JSEN.2021.3085825.
5. Sabato, A., Niezrecki, C., and Fortino, G. (2017). Wireless MEMS-Based Accelerometer Sensor Boards for Structural Vibration Monitoring: A Review. IEEE Sens. J. *17*, 226–235. https://doi.org/10.1109/JSEN.2016.2630008.
6. Wang, S., Wei, X., Zhao, Y., Jiang, Z., and Shen, Y. (2018). A MEMS resonant accelerometer for low-frequency vibration detection. Sens. Actuators Phys. *283*, 151–158. https://doi.org/10.1016/j.sna.2018.09.055.
7. Kok, S.P., Go, Y.I., Wang, X., and Wong, M.L.D. (2024). Advances in Fiber Bragg Grating (FBG) Sensing: A Review of Conventional and New Approaches and Novel Sensing Materials in Harsh and Emerging Industrial Sensing. IEEE Sens. J. *24*, 29485–29505. https://doi.org/10.1109/JSEN.2024.3434351.
8. Rao, Y., Wang, Z., Wu, H., Ran, Z., and Han, B. (2021). Recent Advances in Phase-Sensitive Optical Time Domain Reflectometry (Φ-OTDR). Photonic Sens. *11*, 1–30. https://doi.org/10.1007/s13320-021-0619-4.
9. Yu, Z., Zhang, M., Dai, H., Liu, L., Zhang, J., Jin, X., and Wang, G. (2018). Distributed optical fiber sensing with Brillouin Optical Time Domain Reflectometry based on differential pulse pair. Opt. Laser Technol. *105*, 89–93. https://doi.org/10.1016/j.optlastec.2018.02.037.
10. Dong, Y. (2021). High-Performance Distributed Brillouin Optical Fiber Sensing. Photonic Sens. *11*, 69–90. https://doi.org/10.1007/s13320-021-0616-7.

11. Wang, H., Jiang, L., and Xiang, P. (2018). Improving the durability of the optical fiber sensor based on strain transfer analysis. Opt. Fiber Technol. *42*, 97–104. https://doi.org/10.1016/j.yofte.2018.02.004.

12. Alhussein, A.N.D., Qaid, M.R.T.M., Agliullin, T., Valeev, B., Morozov, O., and Sakhabutdinov, A. (2025). Fiber Bragg Grating Sensors: Design, Applications, and Comparison with Other Sensing Technologies. Sensors *25*, 2289. https://doi.org/10.3390/s25072289.

13. Elsherif, M., Salih, A.E., Muñoz, M.G., Alam, F., AlQattan, B., Antonysamy, D.S., Zaki, M.F., Yetisen, A.K., Park, S., Wilkinson, T.D., and Butt, H. (2022). Optical Fiber Sensors: Working Principle, Applications, and Limitations. Adv. Photonics Res. *3*, 2100371. https://doi.org/10.1002/adpr.202100371.

14. Fan, F.-R., Tian, Z.-Q., and Lin Wang, Z. (2012). Flexible triboelectric generator. Nano Energy *1*, 328–334. https://doi.org/10.1016/j.nanoen.2012.01.004.

15. Zhu, G., Peng, B., Chen, J., Jing, Q., and Lin Wang, Z. (2015). Triboelectric nanogenerators as a new energy technology: From fundamentals, devices, to applications. Nano Energy *14*, 126–138. https://doi.org/10.1016/j.nanoen.2014.11.050.

16. Wang, Y., Du, H., Yang, H., Xi, Z., Zhao, C., Qian, Z., Chuai, X., Peng, X., Yu, H., Zhang, Y., et al. (2024). A rolling-mode triboelectric nanogenerator with multi-tunnel grating electrodes and opposite-charge-enhancement for wave energy harvesting. Nat. Commun. *15*, 6834. https://doi.org/10.1038/s41467-024-51245-5.

17. Zhu, C., Xiang, C., Wu, M., Yu, C., Dai, S., Sun, Q., Zhou, T., Wang, H., and Xu, M. (2024). Recent advances in wave-driven triboelectric nanogenerators: from manufacturing to applications. Int. J. Extrem. Manuf. *6*, 062009. https://doi.org/10.1088/2631-7990/ad7b04.

18. Zhang, R., and Olin, H. (2020). Material choices for triboelectric nanogenerators: A critical review. EcoMat *2*, e12062. https://doi.org/10.1002/eom2.12062.

19. Khan, A., Alam, T., Rashid, M., Mir, S.R., and Hossain, G. (2023). Roll to roll triboelectric fiber manufacturing for smart-textile self-powered sensor and harvester. Nano Energy *111*, 108378. https://doi.org/10.1016/j.nanoen.2023.108378.

20. Yin, B., Wang, L., Liu, J., Gao, S., Zhang, Y., Hong, L., Chen, F., and Tian, M. (2025). Integrated Janus Meta-Fabric via an Interlock Stitch Knitted Structure for Marginal Physiological Signal Monitoring. ACS Appl. Electron. Mater. *7*, 1120–1129. https://doi.org/10.1021/acsaelm.4c01969.

21. Kim, D., Park, J., and Kim, Y.T. (2019). Core–Shell and Helical-Structured Cylindrical Triboelectric Nanogenerator for Wearable Energy Harvesting. ACS Appl. Energy Mater. *2*, 1357–1362. https://doi.org/10.1021/acsaem.8b01931.

22. Yang, Y., Xie, L., Wen, Z., Chen, C., Chen, X., Wei, A., Cheng, P., Xie, X., and Sun, X. (2018). Coaxial Triboelectric Nanogenerator and Supercapacitor Fiber-Based Self-Charging Power Fabric. ACS Appl. Mater. Interfaces *10*, 42356–42362. https://doi.org/10.1021/acsami.8b15104.

23. Zhang, X., Wu, Y., Yu, H., and Menon, C. (2025). Stretchable and Robust All-in-One Tribovoltaic Textile for Sport and Fitness Tracking. Adv. Fiber Mater. *7*, 926–936. https://doi.org/10.1007/s42765-025-00534-9.

24. Guan, X., Xu, B., Huang, J., Jing, T., and Gao, Y. (2022). Fiber-shaped stretchable triboelectric nanogenerator with a novel synergistic structure of opposite Poisson's ratios. Chem. Eng. J. *427*, 131698. https://doi.org/10.1016/j.cej.2021.131698.

25. Zhang, Y., Li, C., Wei, C., Cheng, R., Lv, T., Wang, J., Zhao, C., Wang, Z., Li, F., Peng, X., et al. (2024). An intelligent self-powered life jacket system integrating multiple triboelectric fiber sensors for drowning rescue. InfoMat *6*, e12534. https://doi.org/10.1002/inf2.12534.

26. Lan, B., Wu, F., Cheng, Y., Zhou, Y., Hossain, G., Grabher, G., Shi, L., Wang, R., and Sun, J. (2022). Scalable, stretchable and washable triboelectric fibers for self-powering human-machine interaction and cardiopulmonary resuscitation training. Nano Energy *102*, 107737. https://doi.org/10.1016/j.nanoen.2022.107737.

27. Zhang, C., Wu, S., Bahi, A., Narayana, H., Yang, X., Wang, W., Ke, Y., Yin, X., Zabihi, F., Shao, H., et al. (2024). Tensile-responsive triboelectric yarn based on Janus tubular braided structure for wearable sensing. Nano Energy *131*, 110208. https://doi.org/10.1016/j.nanoen.2024.110208.

28. Xie, L., Chen, X., Wen, Z., Yang, Y., Shi, J., Chen, C., Peng, M., Liu, Y., and Sun, X. (2019). Spiral Steel Wire Based Fiber-Shaped Stretchable and Tailorable Triboelectric Nanogenerator for Wearable Power Source and Active Gesture Sensor. Nano-Micro Lett. *11*, 39. https://doi.org/10.1007/s40820-019-0271-3.

29. Lin, S., Yang, W., Zhu, X., Lan, Y., Li, K., Zhang, Q., Li, Y., Hou, C., and Wang, H. (2024). Triboelectric micro-flexure-sensitive fiber electronics. Nat. Commun. *15*, 2374. https://doi.org/10.1038/s41467-024-46516-0.

30. Sun, Y., Zhang, Y., Shi, H., Wang, S., Liu, J., Luo, Y., Zhang, C., Zhang, K., Li, S.X., and Fan, W. (2025). Hierarchically Engineered Flame-Retardant Triboelectric Yarn Exhibiting Robust Mechanical Performance and Humidity-Boosted Electrical Output for Firefighting Applications. Adv. Sci. *12*, e07673. https://doi.org/10.1002/advs.202507673.

31. Zhou, L., Liu, D., Ren, L., Xue, H., Li, B., Niu, S., Liu, Q., Han, Z., and Ren, L. (2022). Reconfigurable Fiber Triboelectric Nanogenerator for Self-Powered Defect Detection. ACS Nano *16*, 7721–7731. https://doi.org/10.1021/acsnano.1c11569.

32. Wang, X., Guan, X., He, Z., Li, L., Gao, Y., Tan, D., Yin, T., Fu, H., and Xu, B. (2025). Multilayer nanofiber yarns via electrospinning-assisted continuous fabrication for body motion monitoring and intelligent rehabilitation. Nano Energy *142*, 111287. https://doi.org/10.1016/j.nanoen.2025.111287.

33. Chen, W., Fan, W., Wang, Q., Yu, X., Luo, Y., Wang, W., Lei, R., and Li, Y. (2022). A nano-micro structure engendered abrasion resistant, superhydrophobic, wearable triboelectric yarn for self-powered sensing. Nano Energy *103*, 107769. https://doi.org/10.1016/j.nanoen.2022.107769.

34. He, X., Zi, Y., Guo, H., Zheng, H., Xi, Y., Wu, C., Wang, J., Zhang, W., Lu, C., and Wang, Z.L. (2017). A Highly Stretchable Fiber-Based Triboelectric Nanogenerator for Self-Powered Wearable Electronics. Adv. Funct. Mater. *27*, 1604378. https://doi.org/10.1002/adfm.201604378.

35. Zhao, C., Du, T., Ge, B., Xi, Z., Qian, Z., Wang, Y., Wang, J., Dong, F., Shen, D., Zhan, Z., and Xu, M. (2024). Coaxial Flexible Fiber-Shaped Triboelectric Nanogenerator Assisted by Deep Learning for Self-Powered Vibration Monitoring. Small *20*, 2307680. https://doi.org/10.1002/smll.202307680.

36. Yang, Y., Jiang, X., Du, H., Dong, F., Wu, M., Zhao, Q., Du, T., and Xu, M. (2025). Machine learning-enabled triboelectric nanogenerator for self-powered condition monitoring and regulation of USV-ROV umbilical cable. Sens. Actuators Phys. *396*, 117134. https://doi.org/10.1016/j.sna.2025.117134.

37. Dong, K., Deng, J., Ding, W., Wang, A.C., Wang, P., Cheng, C., Wang, Y., Jin, L., Gu, B., Sun, B., and Wang, Z.L. (2018). Versatile Core–Sheath Yarn for Sustainable Biomechanical Energy Harvesting and Real-Time Human-Interactive Sensing. Adv. Energy Mater. *8*, 1801114. https://doi.org/10.1002/aenm.201801114.

38. Zhao, C., Liu, D., Wang, Y., Hu, Z., Zhang, Q., Zhang, Z., Wang, H., Du, T., Zou, Y., Yuan, H., et al. (2022). Highly-stretchable rope-like triboelectric nanogenerator for self-powered monitoring in marine structures. Nano Energy *94*, 106926. https://doi.org/10.1016/j.nanoen.2022.106926.

39. Chen, J., Hu, S., Zhu, S., and Li, T. (2023). Metamaterials: From fundamental physics to intelligent design. Interdiscip. Mater. *2*, 5–29. https://doi.org/10.1002/idm2.12049.

40. Dong, F., Zhu, M., Wang, Y., Chen, Z., Dai, Y., Xi, Z., Du, T., and Xu, M. (2025). AI-enabled rolling triboelectric nanogenerator for bearing wear diagnosis aiming at digital twin application. Nano Energy *134*, 110550. https://doi.org/10.1016/j.nanoen.2024.110550.

41. Li, W., Liu, Y., Wang, S., Li, W., Liu, G., Zhao, J., Zhang, X., and Zhang, C. (2020). Vibrational Triboelectric Nanogenerator-Based Multinode

Please cite this article in press as: Du et al., A stretchable optical-fiber-like triboelectric sensor for monitoring large-scale cable structures, Device (2026), https://doi.org/10.1016/j.device.2026.101079

Self-Powered Sensor Network for Machine Fault Detection. IEEE ASME Trans. Mechatron. *25*, 2188–2196. https://doi.org/10.1109/TMECH.2020.2993336.

42. Wu, H., Xu, X., Xin, C., Liu, Y., Rao, R., Li, Z., Zhang, D., Wu, Y., and Han, S. (2023). Intelligent fault diagnosis for triboelectric nanogenerators via a novel deep learning framework. Expert Syst. Appl. *226*, 120244. https://doi.org/10.1016/j.eswa.2023.120244.

43. Zhang, Z., He, T., Zhu, M., Sun, Z., Shi, Q., Zhu, J., Dong, B., Yuce, M.R., and Lee, C. (2020). Deep learning-enabled triboelectric smart socks for IoT-based gait analysis and VR applications. Npj Flex. Electron. *4*, 29. https://doi.org/10.1038/s41528-020-00092-7.

44. Yun, J., Jayababu, N., and Kim, D. (2020). Self-powered transparent and flexible touchpad based on triboelectricity towards artificial intelligence. Nano Energy *78*, 105325. https://doi.org/10.1016/j.nanoen.2020.105325.